Experiments in Dilution Jet Mixing

J. D. Holdeman*
NASA Lewis Research Center, Cleveland, Ohio
and
R. Srinivasan† and A. Berenfeld‡
The Garrett Turbine Engine Company, Phoenix, Arizona

This paper presents experimental results that extend previous studies on the mixing of a single row of jets with an isothermal mainstream in a straight duct to include the flow and geometric variations typical of combustion chambers in gas turbine engines. The principal conclusions reached from these experiments were: 1) at a constant momentum flux ratio, variations in the density ratio have only a second-order effect on the profiles; 2) a first-order approximation to the mixing of jets with a variable-temperature mainstream can be obtained by superimposing the profiles of jets in an isothermal cross flow on the mainstream; 3) flow area convergence, especially injection wall convergence, significantly improves the mixing; 4) for opposed rows of jets with in-line orifice centerlines, the optimum ratio of orifice spacing to duct height is one-half of the optimum value for single-side injection at the same momentum flux ratio; and 5) for opposed rows of jets with staggered orifice centerlines, the optimum ratio of orifice spacing to duct height is twice the optimum value for single-side injection at the same momentum flux ratio.

Nomenclature

A_j/A_m = orifice-to-mainstream area ratio
$= (\pi/4)/[(S/H_0)(H_0/D)^2]$ for one-side injection
$= (\pi/2)/[(S/H_0)H_0/D)^2]$ for two-side injection
C_d = orifice discharge coefficient
D = orifice diameter
D_j = $(D)(\sqrt{C_d})$
DR = jet-to-mainstream density ratio
$= (\rho_j/\rho_m) = (T_m/T_j)$
H_0 = duct height at injection plane
J = jet-to-mainstream momentum flux ratio
$= (DR)(R)^2$
M = jet-to-mainstream mass flux ratio
$= (DR)(R)$
R = jet-to-mainstream velocity ratio
$= (V_j/U_m)$
S = spacing between orifice centers
T = temperature
T_j = jet exit temperature
T_m = mainstream temperature
U = velocity
U_m = mainstream velocity
V_j = jet velocity
w_j/w_T = jet-to-total mass flow ratio

$$= \frac{(\sqrt{DR})(\sqrt{J})(C_d)(A_j/A_m)}{1+(\sqrt{DR})(\sqrt{J})(C_d)(A_j/A_m)}$$

for all except the variable-temperature mainstream cases
x = downstream coordinate (0 at the injection plane)
y = cross-stream (radial) coordinate (0 at the injection wall)
z = lateral (circumferential) coordinate (0 at the center plane)

Presented as Paper 83-1201 at the AIAA 19th Joint Propulsion Conference, Seattle, Wash., June 27-29, 1983; received July 27, 1983; revision received Nov. 15, 1983. This paper is declared a work of the U.S. Government and therefore is in the public domain.

*Aerospace Engineer, Combustion Branch. Member AIAA.
†Engineering Specialist, Aerothermal Component Design.
‡Senior Engineer, Aerothermal Component Design.

Introduction

THE problem of jets in a cross flow has been rather extensively treated in the literature, to the point that it can almost be called a "classical" three-dimensional flow problem. Although these studies have all contributed to the understanding of the general problem, the information obtained in any given study is determined by motivating application and may not satisfy the specific needs of diverse applications.

Considerations of dilution zone mixing in gas turbine combustion chambers have motivated several previous studies of the mixing characteristics of a row of jets injected normally into a ducted cross flow.[1-11] One factor making the combustor dilution zone application unique is that it is a confined mixing problem with 10-50% of the total flow entering through the dilution jets. The result is that the equilibrium temperature of the exiting flow may differ significantly from that of the entering mainstream flow. To control or tailor the combustor exit temperature pattern, it is necessary to be able to characterize the exit distribution in terms of the upstream flow and geometric variables. This requires that the entire flowfield be either known or modeled.

Empirical correlation of the experimental data can provide an excellent predictive capability within the parameter range of the generating experiments (e.g., see Refs. 4 and 5), but empirical models must be used with caution, or not at all, outside this range. Physical modeling of various levels of sophistication and complexity may be used to obviate this weakness. In this regard, several one-and-two-dimensional integral and differential models of jets in cross flows have been shown to give, for example, trajectory predictions that are in good agreement with experiments. These models may provide insight into the dominant physical mechanism(s) and may predict some of the characteristic parameters well, but they rarely provide sufficient information to quantify the flowfield in the three coordinate directions.

Recently, rapid advances have been made in the capability of computational fluid dynamics models and their application to complex flows such as jet(s) in cross flow.[12,13] However, these models are still in the development and verification stage. They have been shown to be capable of predicting

trends in complex flows, but their capability to provide accurate, quantitive, and grid-independent calculations of these flows has not yet been demonstrated.[13]

Previous Results and the Current Study

The current study was initiated to extend the available experimental data and empirical correlations on the thermal mixing of dilution jets to include geometric and flow variations characteristic of gas turbine combustion chambers. The experiments reported herein are a direct extension of those in Ref. 1 on a single row of jets mixing with an isothermal mainstream in a straight duct. The effect of variations in the orifice size and spacing and the jet-to-mainstream momentum flux ratio[§] on the dimensionless temperature distributions are presented in Ref. 2. From the data of Ref. 1, an empirical model was developed[4,5] for predicting the temperature field downstream of a row of jets mixing with a confined cross flow. An interactive microcomputer program (Apple DOS 3.3) based on this model was used in Ref. 14 to study the effects of separately varying the momentum flux ratio, density ratio, orifice size, and orifice spacing, and to identify the relationship among these parameters which optimizes the mixing. (Although it is recognized that a uniform temperature distribution may not always be desired, "optimum" is used here, as in Refs. 2, 5 and 14 to identify geometries that, for a given flow condition, result in a uniform temperature distribution in a minimum downstream distance.)

The results of these investigations may be summarized as follows: 1) mixing improves with increasing downstream distance; 2) the momentum flux ratio is the most significant flow variable; 3) the effect of the density ratio appeared to be small at constant momentum flux ratios; 4) decreasing the spacing with a constant orifice diameter reduces penetration and increases lateral uniformity; 5) increasing the orifice diameter at a constant spacing-to-diameter ratio improves penetration, but increases lateral nonuniformity; 6) increasing the orifice diameter at a constant orifice spacing (S/H_0) increases the magnitude of the temperature difference, but the jet penetration and profile shape remain similar; 7) if the spacing and momentum flux ratio are correctly coupled, similar jet penetration is obtained over a range of momentum flux ratios, independent of the orifice diameter; and 8) smaller momentum flux ratios (larger spacing) require a greater downstream distance for equivalent mixing.

Variations on the experiments of Ref. 1 considered in the present paper include: the role of the density ratio, variable-temperature mainstream, flow area convergence, and opposed in-line and staggered injection. A more complete presentation of the experimental results and discussion of the empirical modeling performed in this study is given in Refs. 15 and 16. Selected experimental data from these studies are compared with empirical and numerical model predictions in Ref. 17.

Experimental Considerations

Figure 1 shows a flow schematic of the dilution jet test rig. The mainstream temperature and velocity profiles can be varied by adjusting the flow to the profile generator upstream of the test section. Dilution air enters the test section through sharp-edged orifices in the test section walls from the top or bottom, or both. Figure 2 provides more detail of the test sections and orifice configurations used in this study. The height of the test section at the injection plane H_0 was 10.16 cm for all tests. Orifice plate open areas were varied from 2.5 to 20% of the mainstream cross section at the injection location. The primary independent geometric variables are the orifice size and the spacing between adjacent orifices. These are conveniently expressed in dimensionless form as the ratio of the duct height to orifice diameter H_0/D and the ratio of the orifice spacing to duct height S/H_0. The product of these is the orifice spacing-to-diameter ratio S/D, also called the pitch-to-diameter ratio.[9,10] Tests were performed with single-side injection for nonisothermal mainstream conditions and for both symmetric and injection wall convergence (at the rate of 0.5 cm/cm). Both single- and two-side injection tests were performed using the straight duct test section.

The dilution jet mixing characteristics were determined by measuring the temperature and pressure distributions with a vertical rake probe positioned at different axial and lateral stations. This probe had 20 thermocouple elements, with a 20-element total pressure rake and a 20-element static pressure rake located nominally 5 mm (0.05 H_0) on each side of the thermocouple rake. The center-to-center spacing between the sensors on each rake was also 0.05 H_0.

The probe was traversed over a matrix of 48-64 z-x plane survey locations. The flowfield mapping in the z direction was done over a distance equal to 1 or 1.5 times the hole spacing S at intervals of $S/10$. For most tests, the x-y plane containing the orifice centerline (centerplane) was at the center of the span surveyed, i.e., data surveys were from midplane to midplane.

Measurements in the x direction were made at up to five planes with $0.25 \leq X/H_0 \leq 2$. Note that because the objective in this application is to identify the dilution zone configurations that provide a desired mixing pattern within a given combustor length, the downstream stations of interest are defined in intervals of the duct height at the injection location H_0, rather than the orifice diameter D.

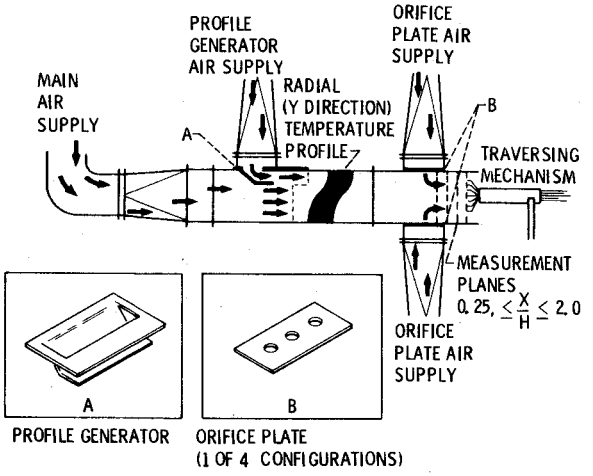

Fig. 1 Dilution jet mixing flow schematic.

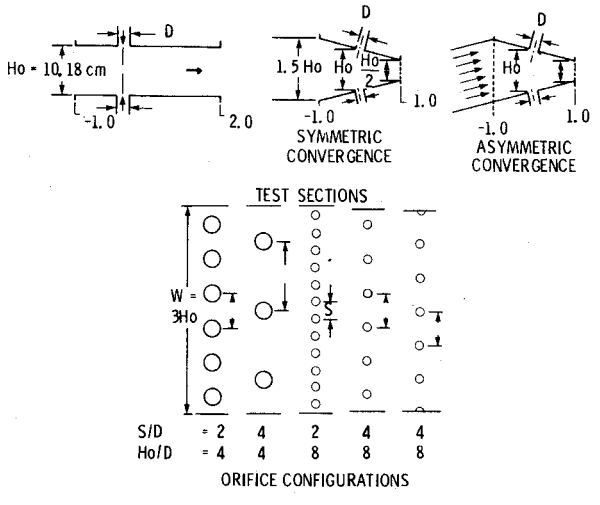

Fig. 2 Test sections and orifice configurations.

Results and Discussion

The measured gas temperature distributions are presented in nondimensional form as

$$\theta = \frac{(T_m - T)}{(T_m - T_j)} \tag{1}$$

Note that $\theta = 1$ if the local temperature is equal to the jet temperature and 0 if the local temperature is equal to the mainstream temperature. The equilibrium θ for any configuration is equal to the fraction of the total flow entering through the dilution jets, w_j/w_T.

The temperature field results are presented in three-dimensional oblique views and as isotherm contours of the temperature difference ratio θ. Typical examples of these are shown in Fig. 3. In these plots, the temperature distribution is shown in planes normal to the main flow direction. The coordinates y and z are, respectively, normal to and along the orifice row in this constant x plane. For clarity and consistency of the visual presentation, the θ distributions are shown over a $2S$ span in the z direction, with the plane between the jets (the midplane) at the edges of the oblique and contour plots. Since for most tests the data were obtained over a span of only one orifice spacing, symmetry was assumed where necessary and the data were reflected across the midplane or centerplane as appropriate to complete the $2S$ span.

The y and z coordinates are shown to scale in the duct cross-sectional schematics on the right of each row in Fig. 3. Note the fourfold decrease in the width of the flow region shown from $S/H_0 = 1$ in the Fig. 3a to $S/H_0 = 0.25$ in Fig. 3c. The profiles and contours in this figure show the relationship between orifice spacing (S/H_0) and momentum flux ratio ($J = (\rho_j V_j^2)/(\rho_m U_m^2)$) that gives optimum mixing for one-side injection.[2,5,14]

In general, the profiles are similar, independent of orifice diameter, when the spacing is inversely proportional to the square root of the momentum flux ratio, i.e.;

$$S/H_0 = C/(\sqrt{J}) \tag{2}$$

For $C = 2.5$, the centerplane profiles are approximately centered across the duct height and approach an isothermal distribution in the minimum downstream distance. Values of C a factor of ≥ 2 larger or smaller correspond to over- or underpenetration, respectively.

The following paragraphs will discuss the experimental results for single-side injection tests with (separately) a nonisothermal mainstream flow, symmetric and injection wall convergence, and opposed in-line and staggered injection in a straight duct. In addition to the variations with geometry, the distributions are examined in terms of the flow variables *DR, R, M,* and *J,* which are the density ratio, velocity ratio, mass flux ratio, and momentum flux ratio, respectively.

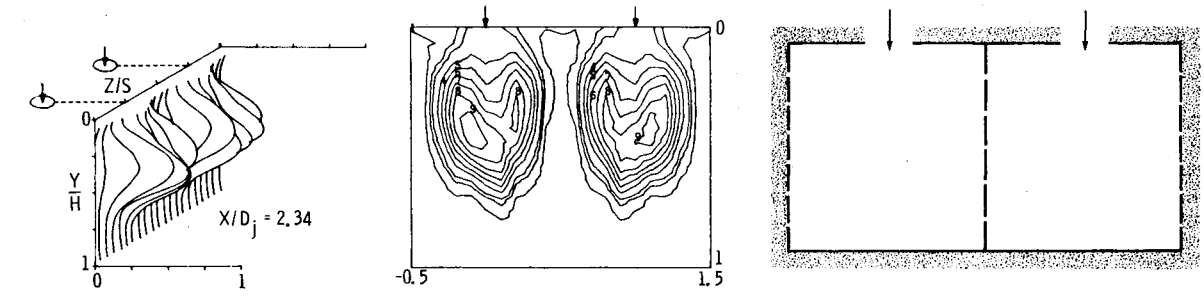

(a) $S/H_0 = 1$, $H_0/D = 4$, $A_j/A_m = .049$, $J = 5.3$, $w_j/w_T = .107$.

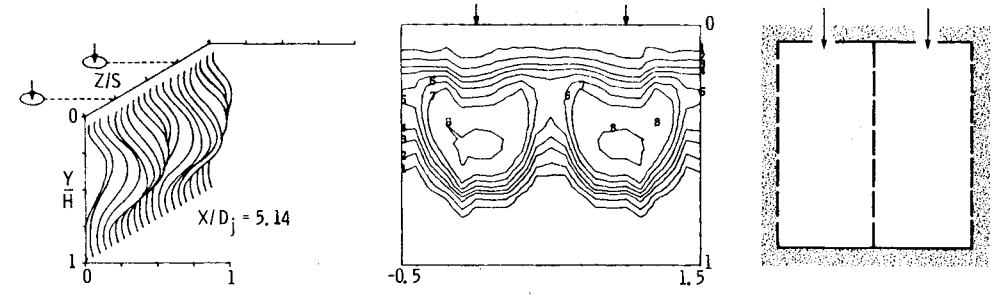

(b) $S/H_0 = .5$, $H_0/D = 8$, $A_j/A_m = .025$, $J = 28.4$, $w_j/w_T = .105$.

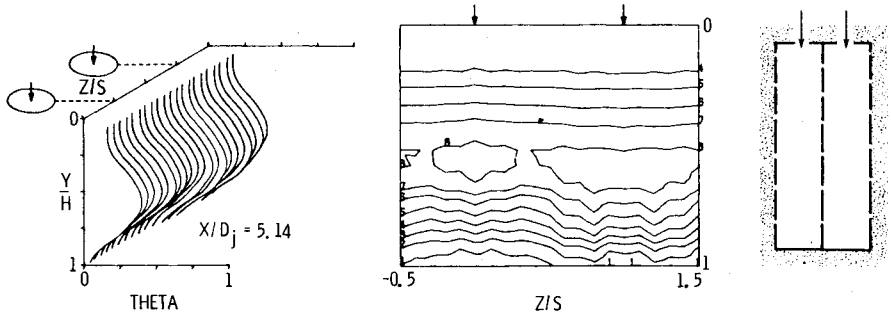

(c) $S/H_0 = .25$, $H_0/D = 8$, $A_j/A_m = .049$, $J = 92.7$, $w_j/w_T = .302$.

Fig. 3 Typical oblique profile plots and isotherm contours at $X/H_0 = 0.5$.

Single-Side Injection

In all of the single-side tests examining the effects of density ratio, variable-temperature mainstream, and flow area convergence, the jets were injected from the top duct wall.

Density Ratio

Figure 4 shows the effect of the density ratio on the θ distributions. These profiles are for an orifice configuration with $S/H_0=0.5$ and $H_0/D=8$ for three different flow conditions. For each of these, the profiles are shown at downstream distances of $X/H_0=0.5$, 1, and 2 from left to right. The profiles in Fig. 4a are for hot jets and an ambient mainstream, whereas those in Figs. 4b and 4c are for ambient jets and a hot mainstream.

In Figs. 4a and 4b, both the momentum flux ratios J and the profiles are similar, even though the density ratio is 0.75 in Fig. 4a and 2.2 in Fig. 4b. The slightly smaller θ levels in Fig. 4a are a result of the smaller jets-to-mainstream mass flow ratio in the case of hot jets. In contrast, the profiles in Fig. 4c show overpenetration, a result of an approximately quadrupled momentum flux ratio. Note, however, that the jet-to-mainstream velocity ratios R are about the same for the hot jets and ambient mainstream case in Fig. 4a, and the ambient jets and hot mainstream case in Fig. 4c.

Figure 5 shows a similar comparison for an orifice plate with the same ratio of orifice spacing to duct height (S/H_0), but with larger holes. The hot jets and ambient mainstream case and the ambient jets and hot mainstream case in Figs. 5a and 5b, respectively, have nearly equal mass flux ratios M, but the jets in Fig. 5b do not penetrate as far into the mainstream due to their lower momentum flux ratio.

All subsequent figures in this paper are for the conditions of ambient jets injected into a hot mainstream with $1.8 \le DR \le 2.3$.

Variable-Temperature Mainstream

The influence of a non-isothermal mainstream flow on the profiles for intermediate momentum flux ratios ($18<J<32$) with $S/H_0=0.5$ and $H_0/D=4$ is shown in Fig. 6. The isothermal mainstream "control" case is shown in Fig. 6a. In Fig. 6b the upstream profile (left frame) is coldest near the injection wall, whereas in Fig. 6c the upstream profile (left frame) is coldest near the opposite wall. The hottest temperature in the mainstream for each case was used as T_m in the definition of θ.

The shape of these distributions suggests modeling them as a superposition of the upstream profile and the θ distributions for jets injected into an isothermal mainstream. However, this gives only a first-order approximation,[15] as there is considerable cross-stream transport of the mainstream fluid caused by blockage that is not taken into account in the superimposed distributions.

Flow Area Convergence

The effect of flow area convergence on the temperature profiles for $S/H_0=0.5$ and $H_0/D=4$, with $J=26$ is shown in Fig. 7. The profiles in Fig. 7a are from the straight-duct test used as the control case in Fig. 6. The profiles in Figs. 7b and 7c are for test sections converging symmetrically and asymmetrically, respectively, to one-half of the injection plane height H_0 in a downstream distance equal to 1 H_0 (i.e., 0.5 cm/cm). Note that the ordinate in these figures is non-

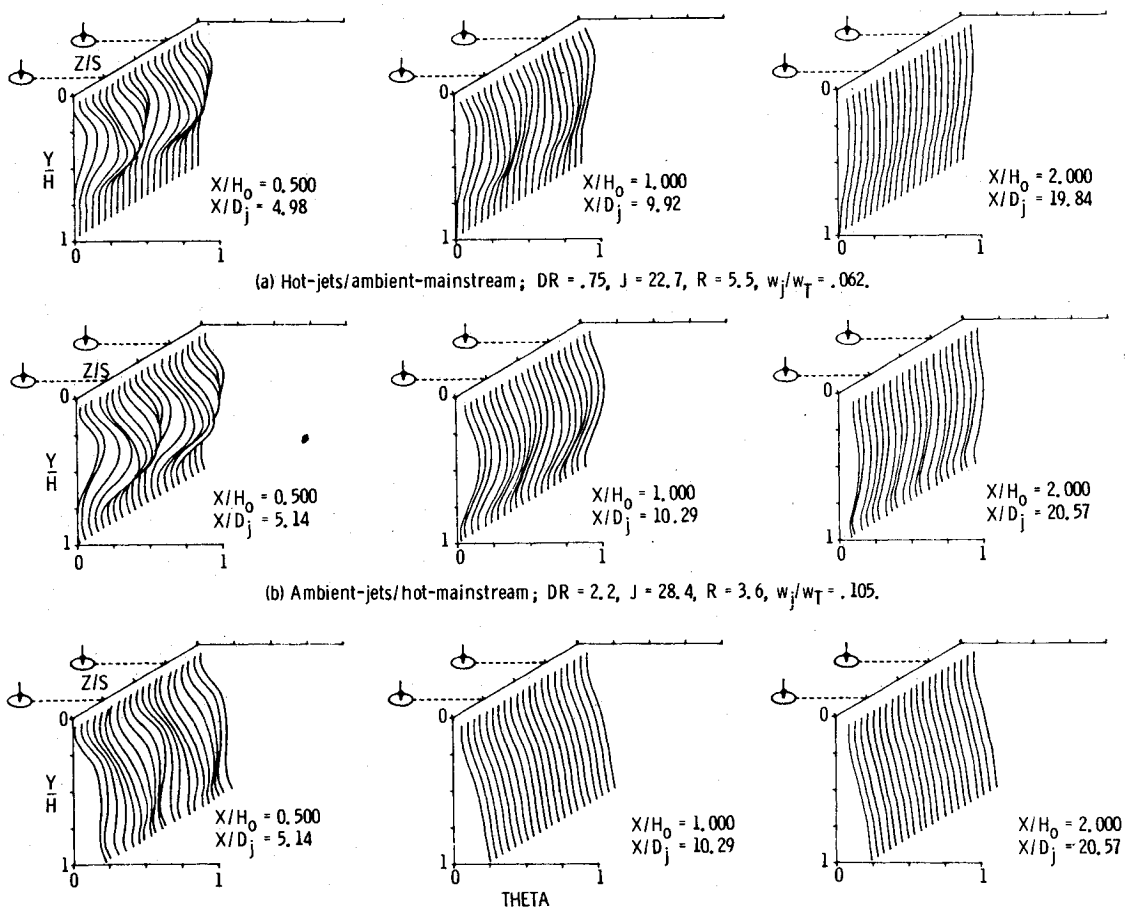

Fig. 4 Effect of density ratio on temperature profiles ($S/H_0=0.5$, $H_0D=8$, $A_j/A_m=0.025$).

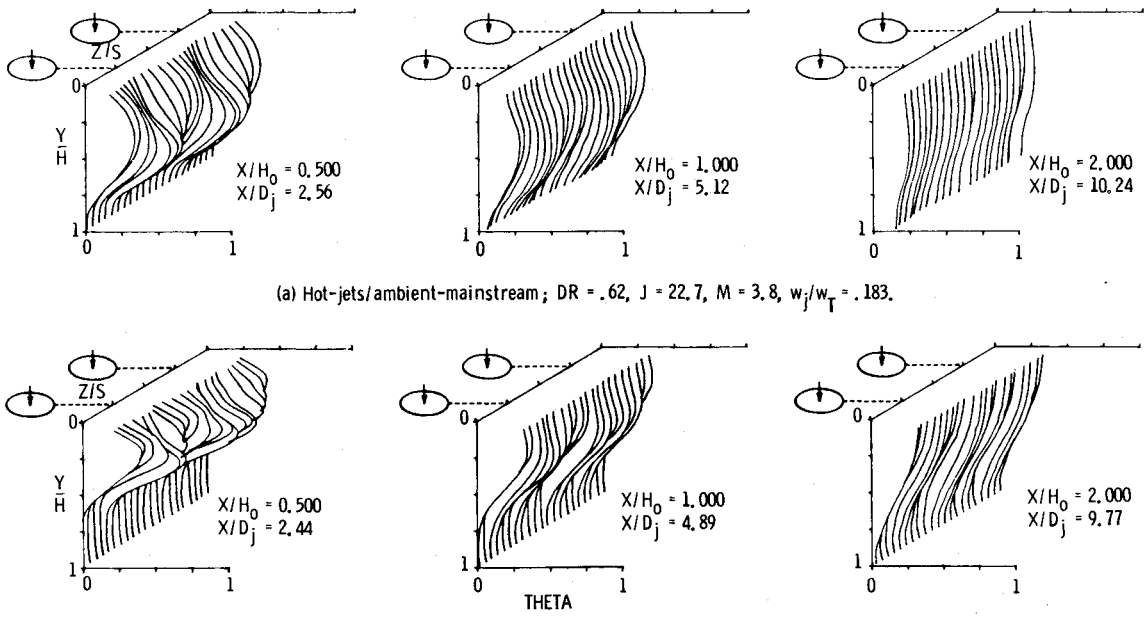

Fig. 5 Effect of density ratio on temperature profiles ($S/H_0 = 0.5$, $H_0 D = 4$, $A_j/A_m = 0.098$).

dimensionalized by the local duct height to remove the influence of streamline convergence on the vertical gradients.

At all downstream locations, the profiles for symmetric convergence (Fig. 7b) are more uniform than the corresponding straight-duct profiles. An even greater effect is seen in the distributions in Fig. 7c where the convergence is asymmetric, with all of the turning on the injection wall. This has a dramatic effect in creating more uniform temperature distributions in both the transverse and lateral directions. Although a detailed analysis is beyond the scope of this paper, the enhanced mixing in the converging sections may be a result of the upstream momentum component of the jet flow and/or the stretching of the strong dual-vortex field characteristic of a jet in cross flow.

Opposing Rows of Jets

The remainder of this paper will discuss the experimental results for two-side injection from opposing rows of jets with: 1) the jet centerlines on the top and bottom directly opposite each other and 2) the jet centerlines on the top and bottom staggered in the z (circumferential) direction. The results of these tests are shown and compared with the single-side results in Figs. 8-11. For each case, a duct cross section is shown to scale to the left of the data.

Opposed-Jet Injection

Figure 8 shows a comparison between single-side and opposed-jet injection with low momentum flux ratios ($5 < J < 8$). For these momentum flux ratios, an appropriate ratio of the orifice spacing to duct height for optimum single-side mixing is approximately one [see Eq. (2)], as shown by the profiles in Fig. 3a.

For opposed-jet injection with equal momentum flux ratios on both sides, the effective mixing height is half the duct height, based on the result[3] that the effect of an opposite wall is similar to that of the plane of symmetry in an opposed-jet configuration. Thus, the appropriate ratio of the orifice spacing to duct height for an opposed-jet injection at these low momentum flux ratios would be about $S/H_0 = 0.5$. Dimensionless temperature disributions downstream of opposed jets with this spacing are shown in Fig. 8b and the two streams do indeed mix very rapidly. Note that since the orifices in Figs. 8a and 8b are the same size, the jet-to mainstream flow ratio is four times greater in the opposed-jet case than in the single-side case.

Table 1 Spacing and momentum flux ratio relationships $C = (S/H_0)(\sqrt{J})$

Configuration	C
Single-side injection	
Underpenetration	≤ 1.25
Optimum	2.5
Overpenetration	≥ 5
Opposed rows of jets	
In-line optimum	1.25
Staggered optimum	5

Figure 8c shows an opposed-jet injection case, at the same momentum flux ratio, in which the orifice area, and hence the jet-to-mainstream flow ratio, has been reduced to that of the single-side case in Fig. 8a. To maintain an equal flow rate, the orifice diameter must be halved, since the opposed-jet cases require twice as many holes in each row compared to the optimum single-side case, and there is injection from both sides.

Figure 9 shows a similar relationship between single-side and opposed jets for intermediate momentum flux ratios, as Fig. 8 showed for low momentum flux ratios. Note that because the momentum flux ratio is larger, the S/H_0 values in Fig. 9 are smaller than the corresponding values in Fig. 8 [see Eq. (2)].

Staggered Jet Injection

Finally, Figs. 10 and 11 show comparisons between single-side and staggered jet injection for intermediate ($21 < J < 27$) and high ($92 < J < 102$) momentum flux ratios, respectively. Since it was found for opposed jet injection that the effective mixing height was half of the duct height, it was assumed for staggered jets that the effective orifice spacing would be half the actual spacing.

This hypothesis is verified by the rapid mixing of the two streams in Figs. 10b and 11b. In both figures, the orifice

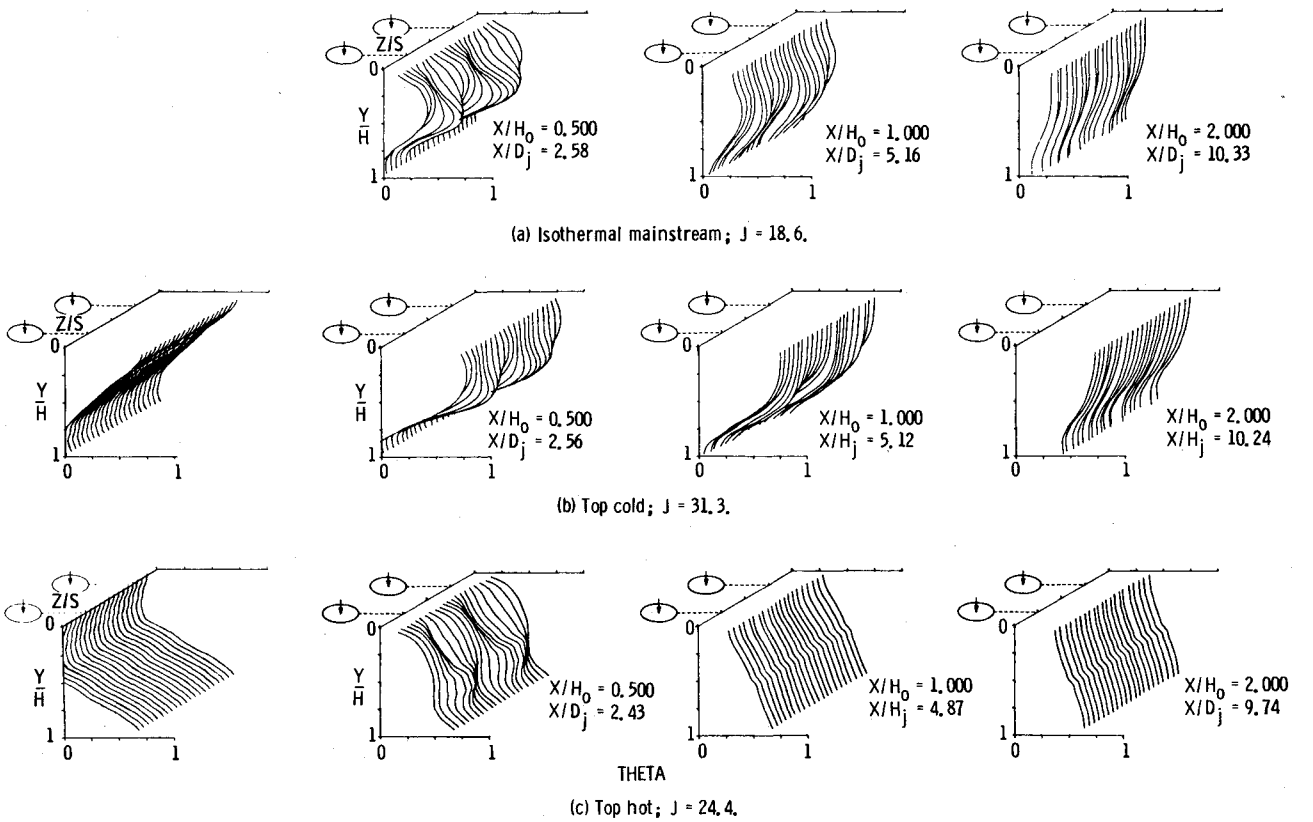

Fig. 6 Influence of non-isothermal mainstream on temperature profiles ($S/H_0 = 0.5$, $H_0/D = 4$, $A_j/A_m = 0.098$).

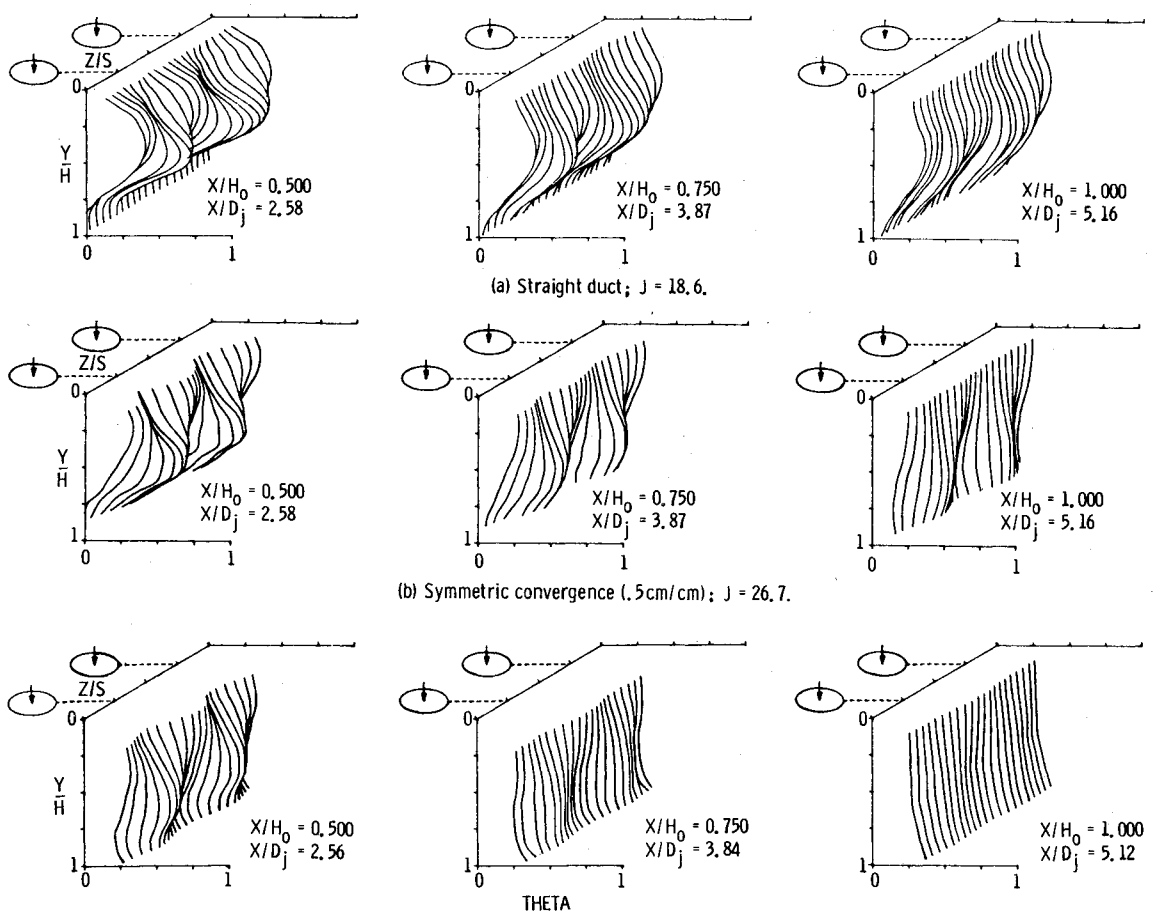

Fig. 7 Influence of flow area convergence on temperature profiles ($S/H_0 = 0.5$, $H_0/D = 4$, $A_j/A_m = 0.098$).

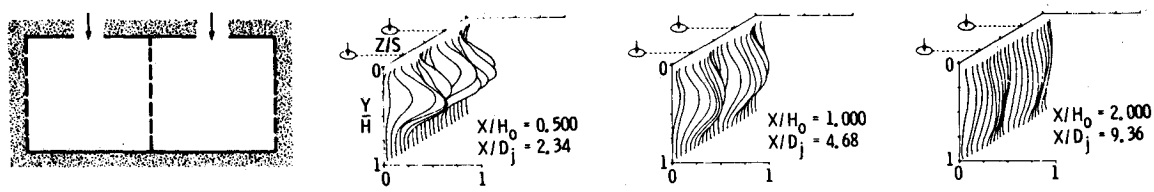

(a) Single-side (top) injection ($S/H_0 = 1$, $H_0/D = 4$, $A_j/A_m = .049$, $J = 5.3$, $w_j/w_T = .107$).

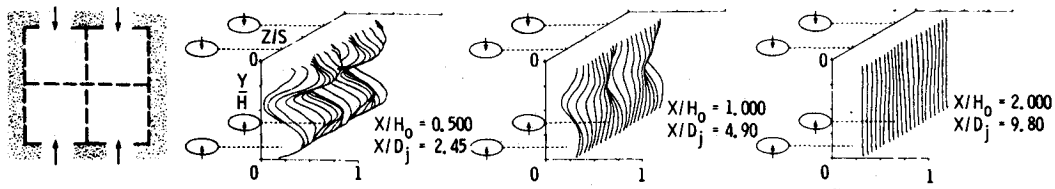

(b) Two-side (opposed) injection ($S/H_0 = .5$, $H_0/D = 4$, $A_j/A_m = .196$, $J = 6.7$, $w_j/w_T = .330$).

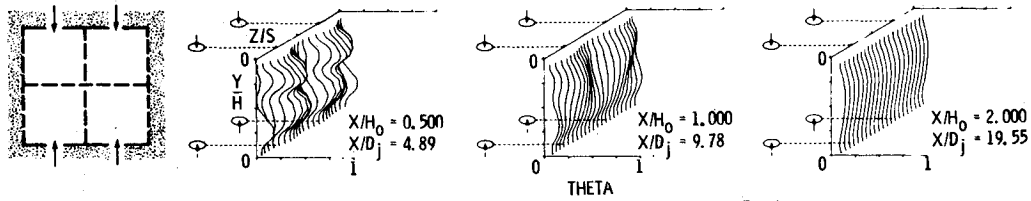

(c) Two-side (opposed) injection ($S/H_0 = .5$, $H_0/D = 8$, $A_j/A_m = .049$, $J = 7.4$, $w_j/w_T = .112$).

Fig. 8 Comparison between single-side and opposed jet injection at low momentum flux ratios.

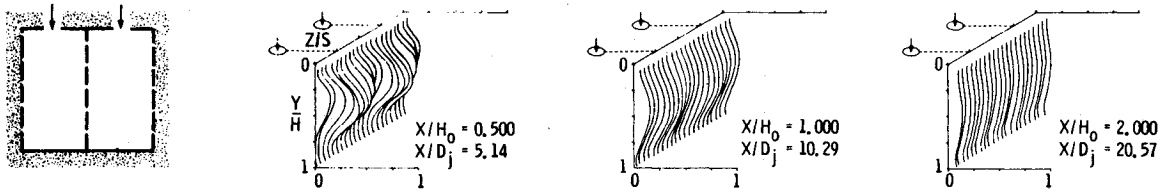

(a) Single-side (top) injection; $S/H_0 = .5$, $A_j/A_m = .025$, $J = 28.4$, $w_j/w_T = .105$.

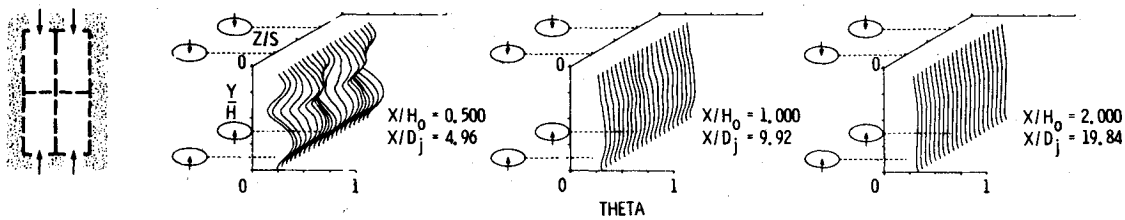

(b) Two-side (opposed) injection: $S/H_0 = .25$, $A_j/A_m = .098$, $J = 25.0$, $w_j/w_T = .318$

Fig. 9 Comparison between single-side and opposed jet injection at intermediate momentum flux ratios ($H_0/D = 8$).

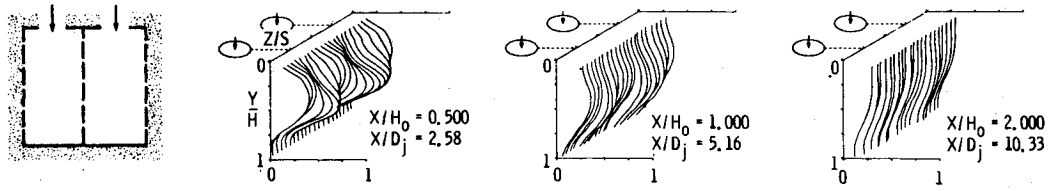

(a) Single-side (top) injection: $S/H_0 = .5$, $J = 18.6$, $w_j/w_T = .271$.

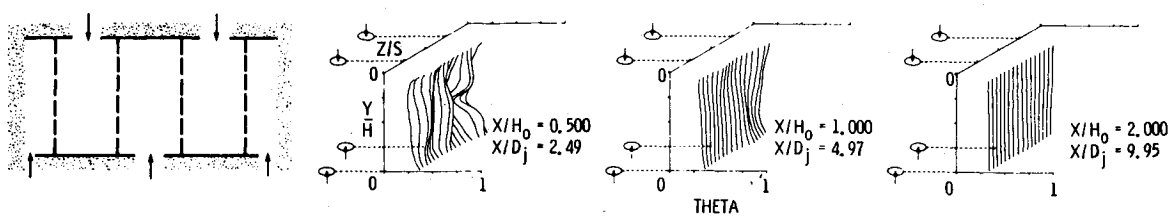

(b) Two-side (staggered) injection: $S/H_0 = 1$, $J = 27.6$, $w_j/w_T = .327$.

Fig. 10 Comparison between single-side and staggered jet injection at intermediate momentum flux ratios ($H_0/D = 4$, $A_j/A_m = 0.098$).

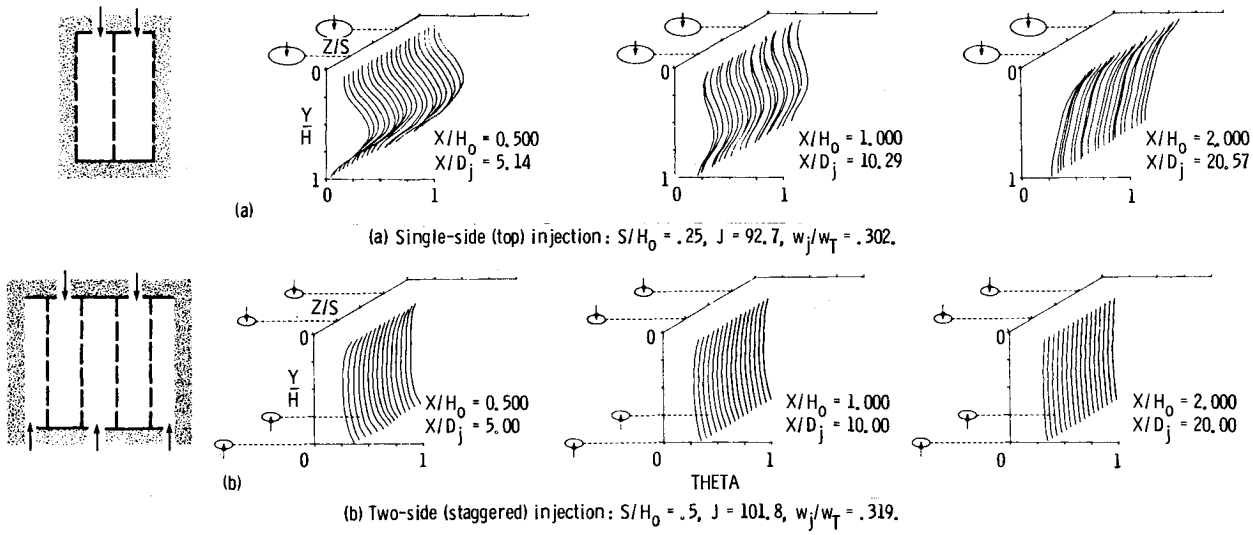

Fig. 11 Comparison between single-side and staggered jet injection at high momentum flux ratios ($H_0/D=8$, $A_j/A_m=0.049$).

spacing for the staggered jets is twice the optimum value for one-side injection at the given momentum flux ratio (Figs. 10a and 11a). That is, a configuration that mixes well with one-side injection performs even better when every other orifice is moved to the opposite wall.

A summary of the spacing and momentum flux ratio relationships for single-side and opposed in-line and staggered jets is given in Table 1.

Summary of Results

The principal conclusions from the experimental results presented herein are:

1) At a constant momentum flux ratio, variations in the density ratio have only a second-order effect on the profiles.

2) A first-order approximation to the mixing of jets with a variable-temperature mainstream can be achieved by superimposing profiles of jets injected into an isothermal mainstream on the variable temperature upstream profile.

3) Flow area convergence, especially injection wall convergence, significantly improves the mixing.

4) For opposed rows of jets, with the orifice centerlines in-line, the optimum ratio of orifice spacing to duct height is one-half of the optimum value for single-side injection at the same momentum flux ratio.

5) For opposed rows of jets with the orifice centerlines staggered, the optimum ratio of orifice spacing to duct height is double the optimum value for single-side injection at the same momentum flux ratio.

References

[1] Walker, R. E. and Kors, D. L., "Multiple Jet Study Final Report," NASA CR-121217, June 1973.

[2] Holdeman, J. D., Walker, R. E., and Kors, D. L., "Mixing of Multiple Dilution Jets with a Hot Primary Airstream for Gas Turbine Combustors," AIAA Paper 73-1249, Nov. 1973 (also NASA TM X-71426, 1973).

[3] Kamotani, Y. and Greber, I, "Experiments on Confined Turbulent Jets in Cross Flow," NASA CR-2392, March 1974.

[4] Walker, R. E. and Eberhardt, R. G., "Multiple Jet Study Data Correlations," NASA CR-134795, 1975.

[5] Holdeman, J. D. and Walker, R. E., "Mixing of a Row of Jets with a Confined Crossflow," *AIAA Journal*, Vol. 15, Feb. 1977, pp. 243-249 (also AIAA Paper 76-48, 1976; NASA TM-71821, 1976).

[6] Cox, G. B. Jr., "Multiple Jet Correlations for Gas Turbine Engine Combustor Design," *Journal of Engineering for Power*, Vol. 98, No. 2, 1976, pp. 265-273.

[7] Cox, G. B. Jr., "An Analytical Model for Predicting Exit Temperature Profile from Gas Turbine Engine Annular Combustors," AIAA Paper 75-1307, Sept. 1975.

[8] Riddlebaugh, S. M., Lipshitz, A., and Greber, I., "Dilution Jet Behavior in the Turn Section of a Reverse-Flow Combustor," AIAA Paper 82-0192, Jan. 1982 (also NASA TM 82776).

[9] Khan, Z. A., McGuirk, J. J., and Whitelaw, J. H., "A Row of Jets in Crossflow," *Fluid Dynamics of Jets with Application to V/STOL*, AGARD-CP-308, Technical Editing and Reproduction. London, 1982.

[10] Atkinson, K. N., Khan, Z. A., and Whitelaw, J. H., "Experimental Investigation of Opposed Jets Discharging Normally into a Cross-stream," *Journal of Fluid Mechanics*, Vol. 115, 1982, pp. 493-504.

[11] Wittig, S. L. K., Elbahar, O. M. F., and Noll, B. E., "Temperature Profile Development in Turbulent Mixing of Coolant Jets with a Confined Hot Cross-Flow," ASME Paper 83-GT-39, March 1983.

[12] Claus, R. W., "Analytical Calculation of a Single Jet in Crossflow and Comparison with Experiment," AIAA Paper 83-0238, Jan. 1983 (also NASA TM 83027, 1983).

[13] Srinivasan, R. et al., "Aerothermal Modeling Program: Phase I Final Report," Garrett Turbine Engine Co., Phoenix, Ariz., Garrett Rept. 21-4742, Aug. 1983 (also NASA CR-168243, 1983).

[14] Holdeman, J. D., "Perspectives on the Mixing of a Row of Jets with a Confined Crossflow," AIAA Paper 83-1200, June 1983 (also NASA TM 83457).

[15] Srinivasan, R., Berenfeld, A., and Mongia, H. C., "Dilution Jet Mixing, Phase 1 Report," Garrett Turbine Engine Co., Phoenix, Ariz., Garrett Rept. 21-4302, Nov. 1982, (also NASA CR-168031).

[16] Srinivasan, R., Coleman, E., and Johnson, R., "Dilution Jet Mixing Program Phase II Report," Garrett Turbine Engine Co., Phoenix, Ariz., Garrett Rept. 21-4804, June 1984 (also NASA CR-174624, 1984).

[17] Holdeman, J. D. and Srinivasan, R., "On Modeling Dilution Jet Flowfields," AIAA Paper 84-1379, June 1984 (also NASA TM 83708, 1984).